Molecular Diagnostics

DOI: 10.1002/ange.201310059

Accurate Zygote-Specific Discrimination of Single-Nucleotide Polymorphisms Using Microfluidic Electrochemical DNA Melting Curves**

*Allen H. J. Yang, Kuangwen Hsieh, Adriana S. Patterson, B. Scott Ferguson, Michael Eisenstein, Kevin W. Plaxco, and H. Tom Soh**

Abstract: *We report the first electrochemical system for the detection of single-nucleotide polymorphisms (SNPs) that can accurately discriminate homozygous and heterozygous genotypes using microfluidics technology. To achieve this, our system performs real-time melting-curve analysis of surface-immobilized hybridization probes. As an example, we used our sensor to analyze two SNPs in the apolipoprotein E (ApoE) gene, where homozygous and heterozygous mutations greatly affect the risk of late-onset Alzheimer's disease. Using probes specific for each SNP, we simultaneously acquired melting curves for probe–target duplexes at two different loci and thereby accurately distinguish all six possible ApoE allele combinations. Since the design of our device and probes can be readily adapted for targeting other loci, we believe that our method offers a modular platform for the diagnosis of SNP-based diseases and personalized medicine.*

Single-nucleotide polymorphisms (SNPs) are important diagnostic indicators for identifying inheritable diseases[1,2] and predicting drug responses.[3] Genetically informed treatment and dosing decisions will require effective platforms for SNP detection that are rapid, portable, and cost effective.[4] Such platforms must also support multiplexed detection and accurately differentiate between homozygous and heterozygous mismatches—a critical factor for many diagnoses.[5,6]

[*] Prof. H. T. Soh
Materials Department
University of California, Santa Barbara
Santa Barbara, CA 93106 (USA)
E-mail: tsoh@engr.ucsb.edu

A. H. J. Yang,[+] K. Hsieh,[+] B. S. Ferguson, M. Eisenstein, Prof. H. T. Soh
Department of Mechanical Engineering
University of California Santa Barbara (USA)

A. S. Patterson, Prof. K. W. Plaxco
Department of Chemistry and Biochemistry and Biomolecular Science and Engineering Program
University of California, Santa Barbara (USA)

[+] These authors contributed equally to this work.

[**] We are grateful for financial support from the Otis Williams Fellowship, the U.S. National Institutes of Health, and the Institute of Collaborative Biotechnologies through the Army Research Office. Microfabrication was carried out in the Nanofabrication Facility at UCSB.

Supporting information for this article is available on the WWW under http://dx.doi.org/10.1002/anie.201310059.

Electrochemical DNA sensors offer robustness, portability, and compatibility with microfluidics and microelectronics,[7,8] and many varieties of electrochemical DNA sensors (as reviewed by Palecek and Bartosik)[9] have been developed for SNP detection, including various enzymatic[10–12] and hybridization-based assays.[13–15] Surface-immobilized, redox-reporter-labeled probes offer many advantages in this arena as they require no exogenous reagents, exhibit low background, and can operate directly in complex mixtures.[16] Innovative probe designs based on triple-stem probes,[17] polarity-switching probes,[18] and base-pair-stacking probes[19] have all proven successful at SNP detection. Unfortunately, none of these sensors have shown the capacity to accurately discriminate heterozygous mismatches, as such samples contain a mixture of matched and mismatched DNA, and these probes cannot accurately resolve the minute differences in hybridization energy. Fluorescence-based, solution-phase methods such as dynamic allele-specific hybridization (DASH) can, in contrast, distinguish homozygous and heterozygous SNPs by means of melting-curve analysis in solution phase.[20] This has spurred interest in integrating melting-curve analysis with electrochemical detection, but these efforts have been confounded by difficulties in obtaining accurate electrochemical and temperature measurements with sufficient speed and resolution.[21–23]

We present a novel microfluidic device that performs electrochemical melting-curve measurements with unprecedented temporal resolution at speeds that enable "real-time" analysis, and can accurately discriminate between homozygous and heterozygous SNP genotypes. Our "microE-DASH" chip employs surface-bound, redox-tagged DNA probes[24] complementary to a SNP-containing target sequence. As we heat the chip, we can obtain a melting curve by continuously measuring changes in the electrochemical signal. Furthermore, microE-DASH can achieve multiplexed detection of homozygous and heterozygous genotypes at multiple loci in a single step by the integration of multiple probes and electrodes within the chip. As a model, we used microE-DASH to genotype two distinct SNP loci associated with the ApoE gene, where specific alleles strongly affect individual risk of late-onset Alzheimer's disease.[25]

MicroE-DASH achieves accurate SNP discrimination by monitoring the thermal melting of duplexes formed by surface-bound probes and their DNA targets in real time (Figure 1 A). The probes are linear, single-stranded DNA, modified with a redox reporter (methylene blue; MB) at their 3′ end and self-assembled onto gold working electrodes

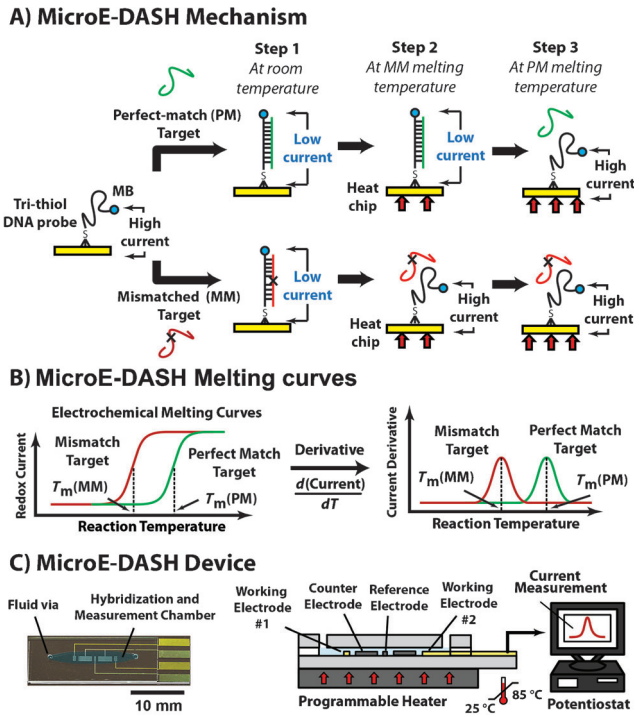

Figure 1. Microelectrochemical dynamic allele-specific hybridization (microE-DASH). A) MicroE-DASH obtains real-time electrochemical melting curves from linear, single-stranded DNA probes complementary to the SNP target. The probes are linked to electrodes through a 5′ tri-thiol anchor with a methylene blue (MB) redox reporter at the 3′ terminus. The flexible unbound probe allows MB to readily approach the working electrode, generating high current. Rigid target–probe duplexes restrict MB–electrode interaction, resulting in a current decrease. Temperature-dependent changes in redox current reveal differences in melting temperature (T_m) between perfectly matched (PM) and mismatched (MM) targets. B) T_m corresponds to the temperature at which the rate of current change is greatest. We can thus determine the T_m by the peak of the first derivative of the redox current as a function of temperature (dI/dT). C) The microE-DASH chip consists of two glass pieces separated by a PDMS gasket; the fluid sample is introduced through a fluidic via drilled through the glass; the entire device is mounted on a programmable Peltier heater. The lower glass piece features two working electrodes, coupled with counter and reference electrodes, which form an electrochemical cell.

through a tri-thiol modification at their 5′ end. In the absence of target, these probes are unstructured and flexible, allowing the MB reporter to readily approach the gold electrode, generating a redox current that can be measured using alternating-current voltammetry (ACV). However, probe–target hybridization decreases the current because the stiffer double-stranded duplex greatly reduces reporter access to the electrode.[26]

To distinguish perfectly matched (PM) targets from those containing single-base mismatches (MM), we increase the temperature until the duplex completely melts. Due to its higher hybridization energy, the PM target (Figure 1 A, top) melts at a higher temperature than the MM target (Figure 1 A, bottom), and microE-DASH can readily distinguish the two by continuously measuring redox current as a function of temperature (Figure 1 B, left). Furthermore, we can accurately determine the melting temperature of the duplex (T_m) by taking the derivative of the current as a function of temperature (dI/dT) as described below (Figure 1 B, right). Heaton et al.[27] and Mahajan et al.[28] have shown that strong DC electric fields can influence DNA duplex formation and dehybridization. However, given the lower magnitude and shorter duration of our AC measurements, we suspect that electric fields have negligible effect on the measured melting temperature of our duplexes.

The microE-DASH chip contains a single reaction chamber that incorporates platinum reference and counter electrodes and two probe-conjugated gold working electrodes to form a multiplexed electrochemical measurement cell (Figure 1 C; see the Supporting Information for fabrication details). The chip is mounted on a Peltier heater, which controls the temperature in a preprogrammed sequence while a potentiostat continuously records the peak redox current from the two working electrodes. Importantly, the chip is designed for minimal thermal resistance, so that the temperature of the electrodes and reaction chamber can equilibrate in seconds (Figure S1). This enables near-real-time acquisition of melting curves, such that the entire assay can be completed within 30 min without the need to return to room temperature for measurement.[22,29] To ensure probe stability, we immobilized them onto the electrodes by means of a 5′-tri-thiol modification.[30] This dramatically improves their thermal stability; mono-thiol probes detach from the electrodes at temperatures as low as 75 °C, whereas tri-thiol probes are stable at temperatures up to 85 °C, maintaining > 99 % of the maximum signal (Figure S2).

As a proof of concept, we designed probes for SNPs within the *ApoE* gene that serve as important clinical diagnostic indicators for Alzheimer's disease.[25] In addition to the normal isoform (ε3), this gene has two variants (ε4 and ε2) arising from SNPs rs429358 (T:C) and rs7412 (C:T), referred to as T1 and T2, respectively, in this work. Carriers of the ε4 allele—and ε4-ε4 homozygotes in particular—exhibit greater risk of developing Alzheimer's.[31] Conversely, the ε2 allele is associated with a reduced likelihood for Alzheimer's.[32] Accurate identification of the six possible allele combinations (Table 1) is thus important for identifying high-risk individuals.

Table 1: *ApoE* genotypes and their associated microE-DASH readout.

Genotype	Alzheimer's risk	T1 melting curve	T2 melting curve
ε3-ε3	normal	PM	PM
ε2-ε2	decreased	PM	MM
ε4-ε4	increased	MM	PM
ε3-ε2	decreased	PM	heterozygous
ε3-ε4	increased	heterozygous	PM
ε2-ε4	normal	heterozygous	heterozygous

We designed probes complementary to the T1 and T2 sequences associated with the ε3 isoform. This allowed us to readily identify homozygotes for ε3, ε2, ε4, or any heterozygous combination of alleles, based on whether T1 and T2 form PM or MM duplexes with their respective probes

(Table 1). We considered three key criteria in designing the probes. First, we ensured that T_m occurs between 45–65 °C, which is sufficiently high for distinguishing secondary melting transitions but within the thermal stability range of the trithiolated probes. Second, we designed probes with minimal secondary structure because self-hybridization can result in complex melting behavior and compete with target hybridization. Finally, we designed the two probes with minimal sequence overlap to minimize potential cross-reactivity. We performed modeling with mfold[33] software to ensure that our probe design satisfied the first two criteria (see the Supporting Information for sequences), and verified their target specificity by immobilizing the probes onto gold electrodes and incubating them with nonmatching targets (i.e., T1 target with T2 probe, and vice versa); this resulted in minimal signal change compared to matched targets (Figure S3).

ACV measurements taken as a function of temperature can precisely track the melting characteristics of DNA targets. To demonstrate this, we hybridized the PM target to the T2 probe and measured the electrochemical current from 25 to 85 °C in 1 °C intervals. We observed a dramatic increase in redox current between 45 and 65 °C (Figure 2A), consistent with the sudden transition expected during melting of the T2–PM duplex. In the absence of target, instead of the sudden current increase expected from a duplex melting transition, we saw a current increase resulting from increased thermal motion of probe molecules at higher temperatures,[23] which in turn results in more frequent interaction between redox reporter molecules and the electrode (Figure S4).

Differences in melting behavior can be directly observed in real time by plotting the peak redox current as a function of temperature. We demonstrated this after challenging T2 probes with PM, MM, or a heterozygous (HET) mixture of PM and MM targets (1:1 ratio) (Figure 2B). We normalized peak-current readings to a 0 to 1 scale using the initial and maximum current values in each run, with five-point averaging to smooth the melt curve (see Methods described in the Supporting Information). As a general trend, we observed clear differences in the half-maximal temperature among the three melting curves. The half-maximal point was reached for the PM target at a higher temperature (61 °C) than the MM target (56 °C), while the curve for the HET mixture fell in between at 58 °C.

To determine accurate T_m values we calculated the derivative of the current with respect to temperature (dI/dT) and defined T_m as the point at which this derivative is largest, analogous to established fluorescence melting approaches.[34] PM and MM targets produced single, distinct peaks with T_m values of 63 °C and 56 °C, respectively (Figure 2C, red and black). This large difference enabled accurate and reproducible detection of SNPs in homozygous samples. Analysis of HET samples is challenging because the resulting dI/dT plot consists of two peaks from the PM and MM targets that can potentially overlap (Figure 2C, blue). To deconvolve the contribution of each probe–target duplex, we adopted an analytical strategy used for extracting peaks from multiple melting curves (see Methods described in the Supporting Information). We applied a curve-fitting algorithm to our single-peak PM and MM melting curves, and determined that

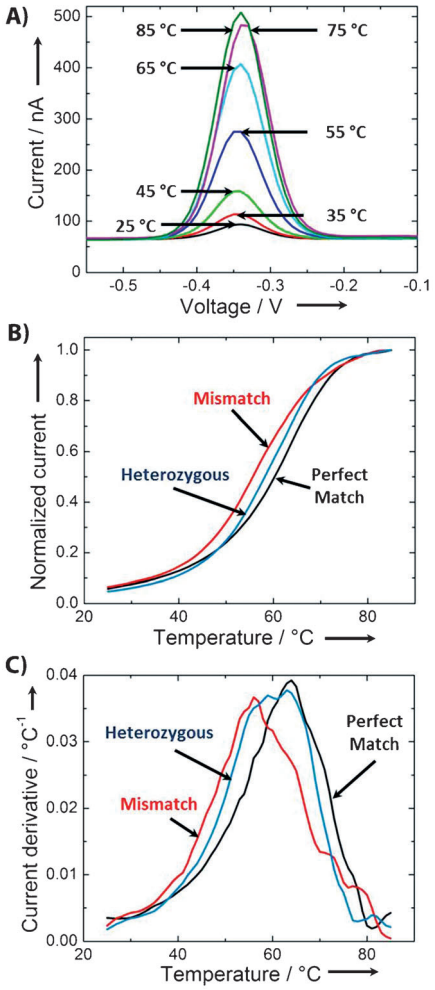

Figure 2. DNA sample genotyping using microE-DASH. A) Peak current traces recorded at 10 °C increments while heating duplexes formed by the T2 probe and PM target reveal T_m-dependent increases in current. B) Plotting the peak currents measured for the T2 probe incubated with PM, MM, and a heterozygous 1:1 mixture of PM and MM at 1 °C increments reveals distinct melting curves for each genotype. Based on the half-maximal current, the PM (black) target forms the most stable duplex with the highest T_m. The MM (red) target forms a less stable duplex with a lower T_m, while the heterozygous sample (blue) exhibits an intermediate T_m. C) By plotting the derivative of the current as a function of temperature (dI/dT) versus temperature, we can determine T_m with a precision of approximately ±1 °C. The target trace from each genotype has a unique peak.

a Lorentzian function yields the best fit to our experimental data (Figure S5).[35,36] When we applied this fit to the T2 heterozygous melting curve (Figure 2C), we identified two curves with peaks at 65.4 °C and 56.6 °C. These correspond well to the measured T_m values of PM and MM, respectively, confirming the validity of this approach.

MicroE-DASH's capacity to simultaneously differentiate multiple homozygous and heterozygous SNP samples enabled us to accurately genotype all six *ApoE* SNP combinations in a single-step assay. We assembled a duplex microE-DASH chip with a different probe immobilized on each of the two sensors, allowing us to simultaneously determine melting

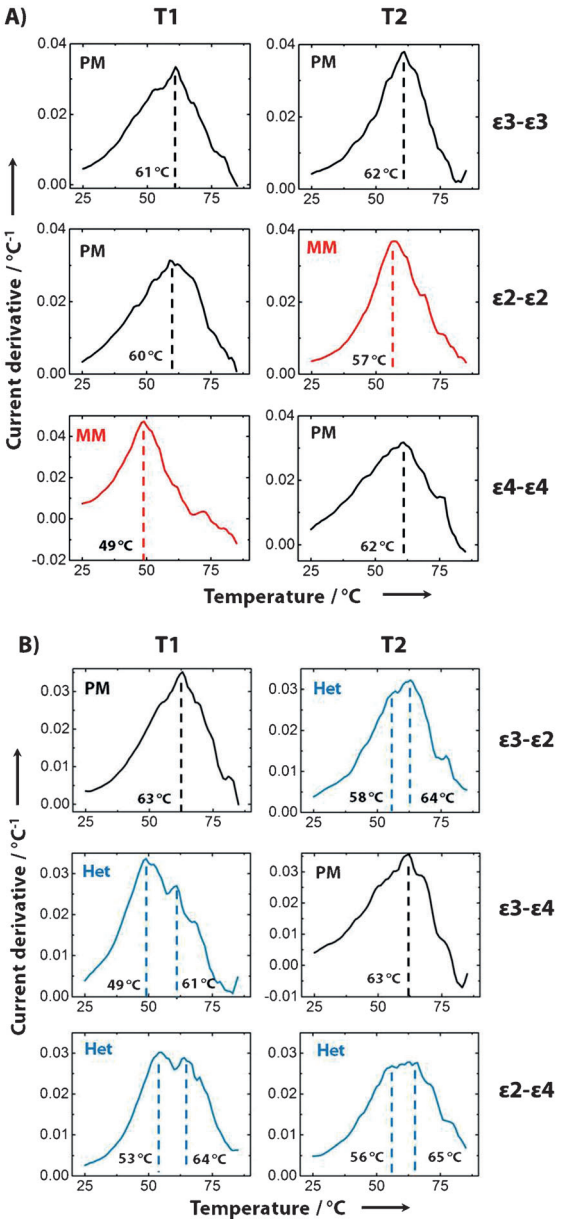

Figure 3. *ApoE* genotyping by multiplexed real-time melting curve analysis. Plots of independent melting curve derivatives from samples containing PCR-length ApoE targets simulating different A) homozygous (PM and MM) and B) heterozygous (Het) genotypes, with the corresponding T_m reported in black. Each row represents a different allele combination, associated with a different response in the T1 or T2 melting curves. Black plots indicate a perfect match between probe and target, whereas red plots indicate SNP mismatch. Blue plots represent profiles with dual peaks arising from heterozygous samples.

temperatures for both T1 and T2. We first obtained melting curves for each of the three homozygous *ApoE* genotypes (Figure 3A). As expected, these samples generated single peaks for both T1 and T2, since SNP mismatches occur in both alleles for any given homozygous genotype. The single-peak T_m values measured in these duplex devices agree with repeated measurements from single-target experiments of T1 (PM: 61 ± 1.5 °C, MM: 50 ± 1 °C) and T2 (PM: 62 ± 0.6 °C, MM: 56 ± 0.6 °C). Furthermore, the shifts in the melting curves observed for the ε2-ε2 and ε4-ε4 samples corresponded with our predictions based on the target–probe mismatches identified in Table 1.

We subsequently used microE-DASH to accurately identify all three possible heterozygous genotypes. We obtained T1 and T2 melting curves as described above, and determined that each heterozygous combination yielded the predicted melting curve shifts (Figure 3B). The ε3-ε2 and ε3-ε4 genotypes resulted in heterozygous melting curves for T2 and T1, respectively, while the ε2-ε4 genotype yielded heterozygous melting curves for both probes. We used deconvolution analysis on the heterozygous melting curves to extract individual T_m values for each target–probe combination, which were in agreement with the PM and MM T_m values obtained from homozygous samples. For example, the T2 melting curve for the ε3-ε2 target yielded peaks of 58 °C and 64 °C, which correspond well with our previous MM and PM T_m measurements of 57 °C and 63 °C, respectively. The ΔT_m for these heterozygous samples matches well with the individually measured single-peak T_m value. This confirms that microE-DASH can accurately report both homozygous and heterozygous genotypes independent of the specific sample composition.

The microE-DASH microfluidic electrochemical SNP biosensor is thus capable of discriminating homozygous and heterozygous samples within 30 min. To demonstrate the potential diagnostic utility of this, we have accurately resolved the six different SNP genotypes commonly associated with *ApoE*, an important diagnostic biomarker for Alzheimer's disease. MicroE-DASH can be readily expanded to incorporate microfluidic PCR and single-strand generation in an integrated device.[37] Since the design of our probes is relatively straightforward, we believe that microE-DASH may offer a modular platform for SNP-based disease diagnostics and personalized medicine.

Received: November 19, 2013
Published online: February 12, 2014

Keywords: DNA · electrochemistry · microfluidics · molecular diagnostics

[1] Y. Suh, J. Vijg, *Mutat. Res. Fundam. Mol. Mech. Mutagen.* **2005**, *573*, 41–53.
[2] S. L. Naylor, *Front. Biosci.* **2007**, *12*, 4111–4131.
[3] J. A. Johnson, W. E. Evans, *Trends Mol. Med.* **2002**, *8*, 300–305.
[4] G. S. Ginsburg, J. J. McCarthy, *Trends Biotechnol.* **2001**, *19*, 491–496.
[5] P. M. Abou-Sleiman, M. M. K. Muqit, N. Q. McDonald, Y. X. Yang, S. Gandhi, D. G. Healy, K. Harvey, R. J. Harvey, E. Deas, K. Hatia, N. Quinn, A. Lees, D. S. Latchman, N. W. Wood, *Ann. Neurol.* **2006**, *60*, 414–419.
[6] I. A. W. van Rijsingen, J. F. Hermans-van Ast, Y. H. J. M. Arens, S. M. Schalla, C. E. M. de Die-Smulders, A. van den Wijngaard, Y. M. Pinto, *Neth Heart J.* **2009**, *17*, 458–463.
[7] T. G. Drummond, M. G. Hill, J. K. Barton, *Nat. Biotechnol.* **2003**, *21*, 1192–1199.
[8] M. Mir, A. Homs, J. Samitier, *Electrophoresis* **2009**, *30*, 3386–3397.
[9] E. Paleček, M. Bartošik, *Chem. Rev.* **2012**, *112*, 3427–3481.

[10] K. J. Feng, J. J. Zhao, Z. S. Wu, J. H. Jiang, G. L. Shen, R. Q. Yu, *Biosens. Bioelectron.* **2011**, *26*, 3187 – 3191.
[11] S. Shin, B. Y. Won, C. Jung, S. C. Shin, D. Y. Cho, S. S. Leec, H. G. Park, *Chem. Commun.* **2011**, *47*, 6611 – 6613.
[12] Y. Huang, J. Zhu, G. Y. Li, Z. C. Chen, J. H. Jiang, G. L. Shen, R. Q. Yu, *Biosens. Bioelectron.* **2013**, *42*, 526 – 531.
[13] R. Ikeda, S. Kobayashi, J. Chiba, M. Inouye, *Chem. Eur. J.* **2009**, *15*, 4822 – 4828.
[14] Y. Wan, R. J. Lao, G. Liu, S. P. Song, L. H. Wang, D. Li, C. H. Fan, *J. Phys. Chem. B* **2010**, *114*, 6703 – 6706.
[15] Y. Wu, R. Y. Lai, *Chem. Commun.* **2013**, *49*, 3422 – 3424.
[16] A. A. Lubin, K. W. Plaxco, *Acc. Chem. Res.* **2010**, *43*, 496 – 505.
[17] Y. Xiao, X. H. Lou, T. Uzawa, K. J. I. Plakos, K. W. Plaxco, H. T. Soh, *J. Am. Chem. Soc.* **2009**, *131*, 15311 – 15316.
[18] K. Hsieh, R. J. White, B. S. Ferguson, K. W. Plaxco, Y. Xiao, H. T. Soh, *Angew. Chem.* **2011**, *123*, 11372 – 11376; *Angew. Chem. Int. Ed.* **2011**, *50*, 11176 – 11180.
[19] E. M. Boon, J. K. Barton, *Bioconjugate Chem.* **2003**, *14*, 1140 – 1147.
[20] W. M. Howell, M. Jobs, U. Gyllensten, A. J. Brookes, *Nat. Biotechnol.* **1999**, *17*, 87 – 88.
[21] A. E. Surkus, G. U. Flechsig, *Electroanalysis* **2009**, *21*, 1119 – 1123.
[22] H. Nasef, V. Beni, C. K. O'Sullivan, *Anal. Methods* **2010**, *2*, 1461 – 1466.
[23] C. H. Wohlgamuth, M. A. McWilliams, J. D. Slinker, *Anal. Chem.* **2013**, *85*, 1462 – 1467.
[24] C. H. Fan, K. W. Plaxco, A. J. Heeger, *Proc. Natl. Acad. Sci. USA* **2003**, *100*, 9134 – 9137.
[25] W. J. Strittmatter, A. D. Roses, *Annu. Rev. Neurosci.* **1996**, *19*, 53 – 77.
[26] T. Uzawa, R. R. Cheng, R. J. White, D. E. Makarov, K. W. Plaxco, *J. Am. Chem. Soc.* **2010**, *132*, 16120 – 16126.
[27] R. J. Heaton, A. W. Peterson, R. M. Georgiadis, *Proc. Natl. Acad. Sci. USA* **2001**, *98*, 3701 – 3704.
[28] S. Mahajan, J. Richardson, T. Brown, P. N. Bartlett, *J. Am. Chem. Soc.* **2008**, *130*, 15589 – 15601.
[29] R. M. Umek, S. W. Lin, J. Vielmetter, R. H. Terbrueggen, B. Irvine, C. J. Yu, J. F. Kayyem, H. Yowanto, G. F. Blackburn, D. H. Farkas, Y. P. Chen, *J. Mol. Diagn.* **2001**, *3*, 74 – 84.
[30] N. Phares, R. J. White, K. W. Plaxeo, *Anal. Chem.* **2009**, *81*, 1095 – 1100.
[31] P. B. Verghese, J. M. Castellano, D. M. Holtzman, *Lancet Neurol.* **2011**, *10*, 241 – 252.
[32] C. Qiu, M. Kivipelto, H. Aguero-Torres, B. Winblad, L. Fratiglioni, *J. Neurol. Neurosurg. Psychiatry* **2004**, *75*, 828 – 833.
[33] W. Vercoutere, S. Winters-Hilt, H. Olsen, D. Deamer, D. Haussler, M. Akeson, *Nat. Biotechnol.* **2001**, *19*, 248 – 252.
[34] G. H. Reed, J. O. Kent, C. T. Wittwer, *Pharmacogenomics* **2007**, *8*, 597 – 608.
[35] I. Belozerova, R. Levicky, *J. Am. Chem. Soc.* **2012**, *134*, 18667 – 18676.
[36] C. J. Wienken, P. Baaske, S. Duhr, D. Braun, *Nucleic Acids Res.* **2011**, *39*, e52.
[37] B. S. Ferguson, S. F. Buchsbaum, J. S. Swensen, K. Hsieh, X. Lou, H. T. Soh, *Anal. Chem.* **2009**, *81*, 6503 – 6508.

